



## ORIGINAL RESEARCH

# Dynamic multi-agent dc-bus reconfiguration in modular motor drives with a stacked polyphase bridge converter

Lynn Verkroost<sup>1,2</sup>  | Alexander Vande Ghinste<sup>1</sup> | Lorrana Faria da Rocha<sup>3</sup> |  
 Jeroen D. M. De Kooning<sup>1,2</sup>  | Frederik De Belie<sup>1,2</sup> | Peter Sergeant<sup>1,2</sup> |  
 Pål Keim Olsen<sup>3</sup> | Hendrik Vansompe<sup>1,2</sup>

<sup>1</sup>Electrical Energy Laboratory, Department of Electromechanical, Systems and Metal Engineering, Ghent University, Ghent, Belgium

<sup>2</sup>Flanders Make@UGent - Corelab MIRO, Ghent, Belgium

<sup>3</sup>Department of Electric Power Engineering, Norwegian University of Science and Technology, Trondheim, Norway

**Correspondence**

Lynn Verkroost.  
 Email: [Lynn.Verkroost@UGent.be](mailto:Lynn.Verkroost@UGent.be)

**Funding information**

Fonds Wetenschappelijk Onderzoek, Grant/Award Number: 3S045319; Flanders Make, Grant/Award Number: ModulAr SBO

**Abstract**

A stacked polyphase bridge converter consists of multiple standard, three-phase two-level voltage source inverters connected in series to the same dc voltage source. The authors present a decentralised and dynamic dc-bus reconfiguration strategy for this type of converter. The innovation of the proposed strategy lies in its ability to isolate or reactivate one of the inverters in the series connection online, even in motoring mode, enabling increased fault tolerance and an extended speed range. Both the required hardware alterations and the multi-agent control strategy are addressed. Its major benefits compared to the state-of-the-art are that only two additional active, unidirectional semiconductor switches are required per inverter, and that the control is based on local computations, local measurements and neighbour-to-neighbour communication only. Hence, the scalability and reliability of the hardware are extended towards the control. Simulations and experimental results on a 4 kW modular axial-flux PMSM prove the feasibility of the concept, and validate that the dc-bus can be reconfigured in 100 ms, without torque interruption.

**KEYWORDS**

AC motor drives, motor drives

## 1 | INTRODUCTION

Modular motor drives (MMDs) are composed of several identical motor modules, fed by dedicated power electronic (PE) modules. They recently gained interest due to their advantageous economies of scales effect, their flexibility, reliability and additional degrees of freedom [1–3]. MMDs that are composed of a multiple of three motor and PE modules—the so-called multi-three-phase machines [4, 5]—are of particular interest, since they can be considered as a group of three-phase winding sets, fed by standard three-phase two-level voltage source inverters (2L-VSIs). From the control point of view, these multi-three-phase machines can make use of the well-consolidated three-phase control strategies, extending the modularity of the hardware to the control as well [6, 7]. The combination of a

three-phase winding set, its 2L-VSI and its dedicated three-phase controller in an MMD can be seen as an agent in a multi-agent system. An agent can hence be regarded as a functional entity that can operate independently from the other agents in the system, but—by allowing communication between the agents—they can also work together to reach a common goal [8–10].

The agents can be fed by multiple dc power sources [11], or they can be connected in series [12, 13] or parallel [9, 10] to a single dc power source. The specific multi-three-phase machine topology that will be studied in this paper, is the so-called stacked polyphase bridge converter [14, 15], depicted in Figure 1. The dc-links of the agents are connected in series to a single dc power supply providing a total dc-bus voltage  $E_{dc}$ , which allows for the use of switches and capacitors with lower voltage ratings without

This is an open access article under the terms of the [Creative Commons Attribution](https://creativecommons.org/licenses/by/4.0/) License, which permits use, distribution and reproduction in any medium, provided the original work is properly cited.

© 2023 The Authors. *IET Electric Power Applications* published by John Wiley & Sons Ltd on behalf of The Institution of Engineering and Technology.

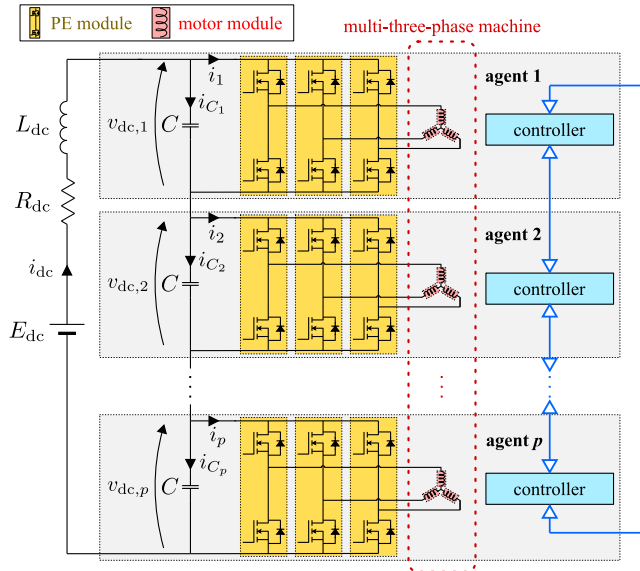


**FIGURE 1** The conventional stacked polyphase bridge converter (without the hardware alterations required for the proposed dc-bus reconfiguration) consists of  $p$  agents, which are connected in series to a single dc-link voltage source  $E_{dc}$ . Each agent comprises three motor modules, three PE modules, and a dedicated controller. A ring communication network allows the agents to exchange information with their closest neighbours.

the need for a power transformer [16]. This feature makes them most suitable for transformerless medium-to-high voltage and power applications (such as offshore wind turbines [17], in the range of 160–320 kV), and automotive applications (such as electric vehicles [18]). Furthermore, when the dc-link capacitor voltage  $v_{dc,x}$  per agent is the same, the stacked polyphase bridge converter draws less dc-link current  $i_{dc}$  from the power source than the configuration in which all the agents are connected in parallel for the same operating points.

However, the stacked polyphase bridge converter topology gives rise to some challenges as well. Small imbalances in the agents may lead to voltage instability, and a breakdown of the complete drive [19]. The authors of Ref. [14] have proven that the voltages  $v_{dc,x}$  over the dc-link capacitors of the agents only remain stable in generating mode. In motoring mode, an active voltage balancing algorithm [13, 14, 20] is required to ensure that the total dc-link voltage  $E_{dc}$  is divided equally among the agents of the converter, and thus to avoid that the breakdown voltages of the semiconductor power switches are exceeded.

Furthermore, the fact that the same dc-link current  $i_{dc}$  runs through all the agents in the series connection introduces a challenge as well. When there is a failure in the 2L-VSI switches or the windings of an agent, and the current path through the three phases of that agent is interrupted, the dc-link current will flow through the agent's dc-link capacitor. In generating mode, this leads to a decrease of the voltage over the capacitor to 0 V, which can safely be by-passed, as is demonstrated in Ref. [17]. However, in motoring mode, this will charge the capacitor and cause over-voltages. In contrast to generating mode, agent isolation in motoring mode has not been covered in the literature.

Although the low dc-link voltage  $v_{dc,x}$  per agent is regarded as one of the major benefits of the stacked polyphase bridge converter (as it reduces its component's voltage ratings), it is also one of its drawbacks. This is especially the case when the converter is used in combination with a permanent magnet synchronous machine (PMSM). After all, the dc-link voltage per agent imposes a limit on the back electromotive force (back-EMF), and hence the speed of the electric machine. In the literature, multiple strategies are considered to increase the speed range, such as field-weakening [21, 22], variable flux machines [23, 24] and winding reconfiguration strategies [25, 26]. These reconfiguration strategies either reduce the back-EMF, or increase the available voltage over a machine winding. The main issues of the existing reconfiguration strategies are the high number of additional active—and sometimes even bidirectional—switches that are required, and the occurrence of a short torque interruption during reconfiguration.

## 1.1 | Key challenges

To summarise, modular motor drives fed by a stacked polyphase bridge converter are still facing the challenge that a faulty agent cannot be isolated from the series connection in motoring mode. Hence, a single failing agent forces the complete system to shut down. Furthermore, the limited dc-link voltage per agent imposes a limit on the back-EMF (and hence the speed) of the MMD. The main issues of the state-of-the-art reconfiguration strategies that deal with this speed limit are the high number of additional active (bidirectional) switches that are required, and the occurrence of a short torque interruption during reconfiguration. Therefore, in this paper, a multi-agent dc-bus reconfiguration strategy is proposed, which enables to isolate and reactivate an agent in the series connection of the stacked polyphase bridge converter in motoring mode, while keeping the capacitor voltages over the active agents balanced. The proposed strategy is able to isolate a faulty agent in motoring mode, and to increase the drive's speed range for traction applications. At low speed, all the agents are connected in series to produce a high torque. At high speed, agents are disconnected in order to divide the total dc-link voltage over less agents. Figure 2 illustrates the speed–torque characteristic that can be obtained in this way. However, the advantage that all the semiconductor switches and capacitors can have lower voltage ratings is lost in this case.

The proposed reconfiguration strategy exhibits multiple advantages, which address the remaining challenges:

- the reconfiguration strategy requires only two additional active, unidirectional switches per agent (which are indicated in Figure 3);
- the reconfiguration is dynamic, that is, the torque is not interrupted when an agent is isolated or reactivated, and the isolation and activation take place in 100 ms (making it competitive with for instance the gearbox of a Bugatti Veyron DSG [27]);

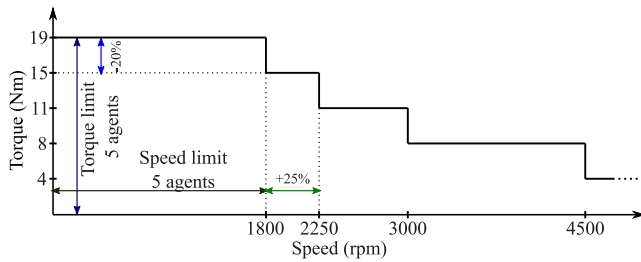


**FIGURE 2** Speed–torque characteristic of an MMD with a reconfigurable stacked polyphase bridge converter with five agents, without using field-weakening. At low speeds, all agents are connected in series to produce maximum torque. When the speed (and hence the back-EMF) becomes too high for the dc-link voltage per agent, the agents are one by one disconnected from the series connection. Per agent that is disconnected, the maximum available torque decreases, but the dc-link voltage per agent increases, allowing for a speed range extension.

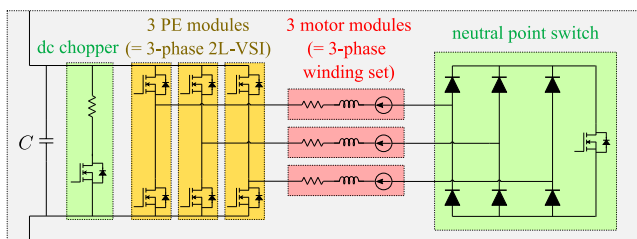


**FIGURE 3** Adapted agent topology, required for agent isolation and activation in the series connection of the converter. Apart from the three-phase winding set and 2L-VSI, the agent is also equipped with a dc chopper and neutral point switch.

- the strategy is completely decentralised, that is, there is no need for a central or master controller (which is a single point of failure), and only the agent that is isolated or reactivated needs to make alterations to its control strategy;
- the strategy can be adopted for any number of agents in the series connection, without a complete redesign of the control scheme;
- the applied active voltage balancing algorithm does not require an additional voltage sensor to measure the total dc-bus voltage  $E_{dc}$ .

Although the proposed dc-bus reconfiguration strategy can be applied to isolate a faulty agent, or to extend the speed range of an MMD, the focus of this paper is on the reconfiguration procedure itself. More specifically, this means that the incentive for an agent to isolate or activate itself comes from an external command, and not from the detection of a fault, or from the operating point. Furthermore, the current and speed set-points are kept constant during reconfiguration. As a result, the speed will remain the same, but the torque will decrease when an agent is isolated, and rise again when an agent is reactivated. Although out of scope for this paper, these torque changes can be avoided by letting the agents redistribute the

torque demand among the remaining active agents in a decentralised way as explained in Refs. [9, 10].

## 1.2 | Outline

Section 2 gives an elaborate definition of the MMD architecture presented in this paper, followed by an explanation of the complete decentralised multi-agent voltage balancing control scheme in Section 3. The procedures for agent isolation and activation are discussed in Sections 4 and 5, respectively. The case study presented in Section 6 validates the complete reconfiguration strategy by means of both simulations and experimental results for a multi-three-phase 4 kW segmented armature torus axial-flux permanent magnet synchronous machine (AFPMSM) with surface-mounted permanent magnets consisting of five agents.

## 2 | MODULAR MOTOR DRIVE ARCHITECTURE

A modular motor drive is created by segmenting the drive in  $n$  pole drive units (PDUs), each consisting of a motor module (which is a stator core segment and its corresponding winding), fed by a dedicated power electronic converter module (which comprises a half-bridge inverter leg and a phase current measurement in this work).

The motor and PE modules of modular motor drives that consist of a multiple of three PDUs (i.e.  $n = 3 \times p$ ) can be grouped into three-phase winding sets, fed by standard three-phase 2L-VSIs. Each three-phase set is connected in a separate neutral point, is equipped with a voltage sensor to measure its local dc-link voltage  $v_{dc,x}$ , and is controlled by means of a dedicated (micro) controller. A set of three motor modules, three PE modules, a voltage sensor and its controller is called an agent, as depicted in Figure 1. The PDUs are arranged in such a way that they have a phase shift of  $2\pi/3$  electrical radians within an agent, and that the PDUs of neighbouring agents are shifted with  $2\pi/n$  electrical radians in this work. The  $p$  three-phase 2L-VSIs of the agents are connected in series to a single dc power supply providing the total dc-link voltage  $E_{dc}$ , giving rise to a so-called stacked polyphase bridge converter. A ring communication network is established between the agents, making it possible for each agent to communicate with its two closest neighbours (i.e. agent  $x \in \{1, \dots, p\}$  can communicate with agent  $x - 1 \in \{1, \dots, p\}$  and agent  $x + 1 \in \{1, \dots, p\}$ ).

However, the standard version of an agent, as depicted in Figure 1 and described above, is not adequately equipped to be isolated from the series connection, nor to be reactivated afterwards. Figure 3 shows the adaptations that are required for this purpose. Next to the power electronic switches present in the 2L-VSI, two additional active switches are required per agent: one as part of a neutral point switch, and one as part of a

dc chopper. The purpose and functioning of these two additional hardware components will be elaborated upon in Sections 4.2 and 4.3, respectively.

### 3 | MULTI-AGENT VOLTAGE BALANCING CONTROL

An important drawback of the stacked polyphase bridge converter is the need for an active voltage balancing control in motoring mode. The goal of this voltage balancing algorithm is to ensure that the total dc-link voltage  $E_{dc}$  is divided equally among the active agents. In this work, a completely decentralised multi-agent voltage balancing algorithm is used for this purpose, which is based on the algorithm presented in Ref. [13]. This algorithm avoids the need for a central voltage sensor to measure the total dc-bus voltage  $E_{dc}$ , as this is an additional voltage sensor and a single point of failure. Furthermore, it does not rely on a central or master controller (which is also a single point of failure) to keep track of the number of active agents  $p_{act}$  and to generate the voltage references  $E_{dc}/p_{act}$  for these active agents. The multi-agent algorithm hence extends the fault-tolerance, reliability and scalability of the modular hardware towards the control. The multi-agent voltage balancing

algorithm consists of three sub-algorithms, as schematised in Figure 4:

1. a dynamic average consensus algorithm to determine the voltage references  $\bar{v}_{dc,x}$  for the active agents in a decentralised way,
2. the voltage balancing algorithm itself, which makes sure that the dc-link voltages  $v_{dc,x}$  of the active agents follow their references  $\bar{v}_{dc,x}$  by adding small increments to the current component references of the agents,
3. a decentralised current control algorithm that regulates the current components of the agents to the current set-points computed by the voltage balancing algorithm.

These three sub-algorithms are discussed in more detail in the following sections.

#### 3.1 | Dynamic average consensus for voltage reference generation

The controller of each agent conducts a dynamic average consensus algorithm to compute its own voltage reference. It is required that

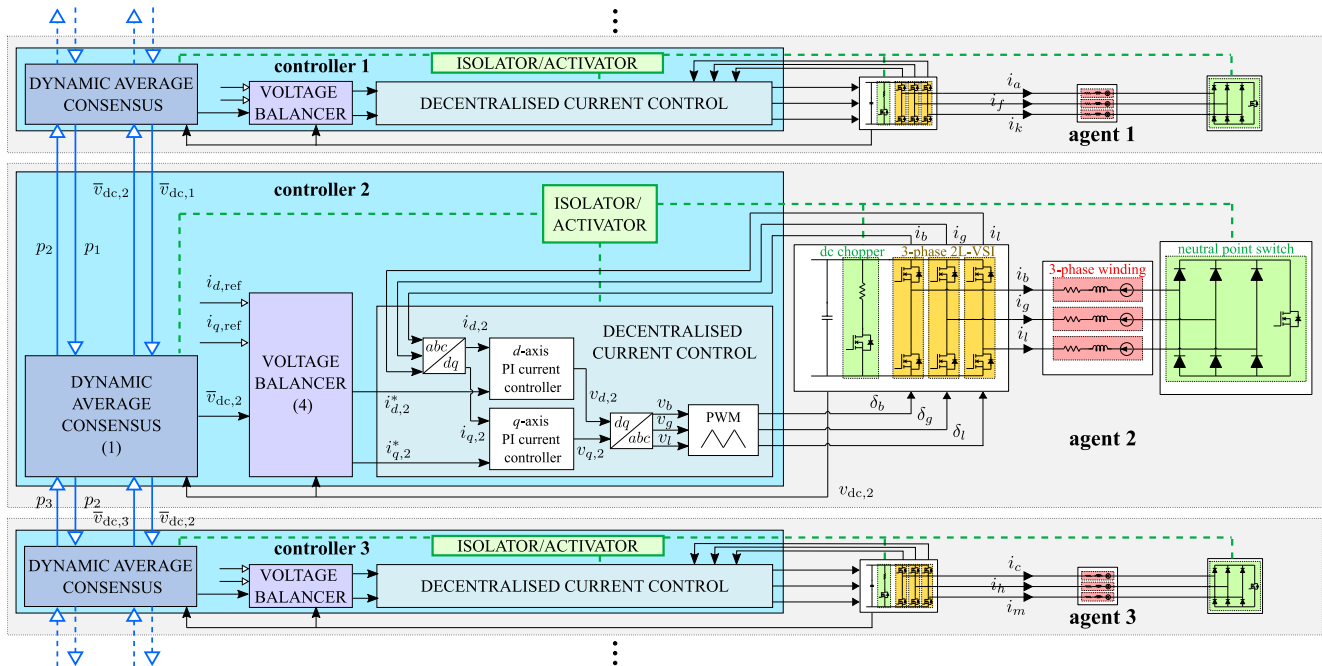


**FIGURE 4** Detail of the controller of agent 2. In general, each agent  $x$  measures the voltage  $v_{dc,x}$  over its 2L-VSI and communicates the parameters  $\bar{v}_{dc,x}$  and  $p_x$  with its two closest neighbours (which are agent 1 and agent 3 for agent 2), in order to compute the average of the voltages over all the agents by means of the dynamic average consensus algorithm (1) of Section 3.1. This average voltage  $\bar{v}_{dc,x}$  is used as the voltage reference for the voltage balancer (4) of agent  $x$ , which is explained in Section 3.2. The voltage balancer outputs agent-specific current set-points  $i_{d,x}^*$  and  $i_{q,x}^*$ , which are then fed to the independent, three-phase field oriented current controller of that agent, which is elaborated upon in Section 3.3. This decentralised current controller requires only information of agent  $x$  itself, and determines the duty cycles  $\delta$  for the three-phase 2L-VSI which feeds the three concentrated windings of this agent  $x$ . A three-phase current measurement provides feedback to the decentralised current controller. Each agent is able to isolate or reactivate itself independently from the other agents, by adapting its dynamic average consensus algorithm, and by steering the switching of its 2L-VSI, its dc chopper, and its neutral point switch. When an agent isolates itself from the series connection, it first opens all the switches of its 2L-VSI and its neutral point switch to eliminate the back-EMF, after which it discharges its capacitor by means of its dc chopper. To reactivate itself, the agent uses its dc chopper to recharge its capacitor, after which its neutral point switch is closed again. The 2L-VSI can start switching according to the duty cycles coming from the decentralised controller again.



- each agent  $x$  knows from itself whether it is active or not,
- each agent  $x$  has access to its own local voltage measurement  $v_{dc,x}$ ,
- each agent  $x$  can communicate with its two closest neighbours (i.e. agent  $x - 1$  and  $x + 1$ ) by means of a ring communication network.

The discrete-time dynamic average consensus algorithm proposed in Ref. [28] is chosen in this work, because it is robust to initial conditions, and it is able to track the average of constant (or slowly varying) input signals with zero (or small) steady-state error. For each agent  $x$ , the output  $\bar{v}_{dc,x}$  of this consensus algorithm tracks the time-varying average  $\sum_{y=1}^{p_{act}} v_{dc,y} / p_{act} \approx E_{dc} / p_{act}$  of the local voltage measurements of all the active agents, which will serve as the reference voltage for the voltage balancing algorithm of agent  $x$ .

At each discrete time instant  $k$  (with the voltage balancer's update period  $T_{vb} = 1/f_{vb}$  between subsequent time instants), all the agents are assumed to have exchanged their variables  $p_x$  and  $\bar{v}_{dc,x}$  with their two closest neighbours, and to update their variables as follows [13, 28, 29]:

$$q_x(k+1) = \rho q_x(k) + k_p \left\{ \left[ \bar{v}_{dc,x}(k) + p_x(k) \right] - \frac{1}{2} \left[ \bar{v}_{dc,x-1}(k) + p_{x-1}(k) \right] - \frac{1}{2} \left[ \bar{v}_{dc,x+1}(k) + p_{x+1}(k) \right] \right\}, \quad (1a)$$

$$p_x(k+1) = p_x(k) + k_i \left\{ \bar{v}_{dc,x}(k) - \frac{1}{2} \bar{v}_{dc,x-1}(k) - \frac{1}{2} \bar{v}_{dc,x+1}(k) \right\}, \quad (1b)$$

$$\bar{v}_{dc,x}(k+1) = v_{dc,x,f}(k) - q_x(k+1) \quad (1c)$$

with

$$v_{dc,x,f}(k) = \alpha v_x(k) + [1 - \alpha] v_{dc,x,f}(k-1), \quad (2)$$

and

$$v_x(k) = \begin{cases} v_{dc,x}(k), & \text{if agent } x \text{ is active;} \\ \frac{\bar{v}_{dc,x-1}(k) + \bar{v}_{dc,x+1}(k)}{2}, & \text{if agent } x \text{ is not active.} \end{cases} \quad (3)$$

$q_x$  and  $p_x$  are internal state variables of agent  $x$ , and  $\alpha$  is a filtering constant. The filtering of the voltage sensor outputs by means of (2) avoids that the voltage reference  $\bar{v}_{dc,x}$  is heavily influenced by measurement noise, and, according to Ref. [14], it enhances the stability of the voltage balancer. Analytical expressions for the parameters  $\rho$ ,  $k_p$  and  $k_i$  can be found in Refs. [13, 28, 29], which result in the fastest convergence of the consensus algorithm.

## 3.2 | Active voltage balancing

The authors of Refs. [13, 14] propose to stabilise the dc-link voltages by adding a stabilisation term with a gain  $g$  to the original current component references  $i_{d,ref}$  and  $i_{q,ref}$  at each update period  $T_{vb}$ :

$$i_{d,x}^*(k) = i_{d,ref}(k) + g i_{d,ref}(k) [v_{dc,x}(k) - \bar{v}_{dc,x}(k)], \quad (4a)$$

$$i_{q,x}^*(k) = i_{q,ref}(k) + g i_{q,ref}(k) [v_{dc,x}(k) - \bar{v}_{dc,x}(k)]. \quad (4b)$$

When the capacitor voltage  $v_{dc,x}$  of agent  $x$  is larger than its reference  $\bar{v}_{dc,x}$ , the current set-points of this agent increase. More current will be drawn into the windings of this agent, resulting in a rise in the power  $P_x$  of this agent as well:

$$P_x = \frac{3}{2} \left[ R_s (i_{d,x}^2 + i_{q,x}^2) + \omega \Psi_m i_{q,x} + \omega (L_d - L_q) i_{d,x} i_{q,x} \right],$$

with  $R_s$  ( $\Omega$ ) the stator winding resistance,  $\Psi_m$  (Wb) the permanent magnet flux linkage,  $L_d$  and  $L_q$  (H) the stator winding inductances, and  $\omega$  (rad/s) the electrical speed. If the inverter losses can be neglected, the inverter current  $i_x$  of agent  $x$  (as indicated in Figure 1) increases as well, according to the following equation:

$$i_x = \frac{P_x}{v_{dc,x}}.$$

As the dc-link capacitance  $C$  (F), the capacitor voltage  $v_{dc,x}$  and the inverter current  $i_x$  have the following relation:

$$C \frac{dv_{dc,x}}{dt} = i_{dc} - i_x,$$

this rise in  $i_x$  allows for a decrease in  $v_{dc,x}$ . The inverse happens when  $v_{dc,x}$  is smaller than its reference  $\bar{v}_{dc,x}$ . The magnitude of the current vector  $\sqrt{i_{d,x}^{*2} + i_{q,x}^{*2}}$  is limited to  $i_{max}$ , and  $i_{q,x}^* > 0$  to ensure motoring mode.

Due to the fact that the stabilisation term in (4) introduces additional stator current ripple, and the fact that additional reactive power is required to balance the capacitor voltages of the agents, the efficiency of the stacked polyphase bridge converter is slightly lower than for the configuration in which all the agents are connected in parallel to the same dc power source.

## 3.3 | Decentralised current control

Each agent  $x$  regulates its current components  $i_{d,x}$  and  $i_{q,x}$  towards the set-points  $i_{d,x}^*$  and  $i_{q,x}^*$  generated by the voltage balancer by means of an independent three-phase vector PI controller with sampling frequency  $f_s$ . The PI parameters  $K_p$  and  $K_i$  (which are the same for all  $p$  agents, and remain unchanged when an agent is isolated or activated) are tuned in

such a way that a  $q$ -current set-point amplitude change in agent  $x$  does not deviate the current components  $i_{d,y}$  and  $i_{q,y}$  in the other agents  $y$  with more than 13% of the magnitude of the  $q$ -current set-point change. For this purpose, a multi-variable frequency analysis as described in Ref. [6] is conducted, which takes into account the internal magnetic coupling between the agents.

## 4 | AGENT ISOLATION

This section will cover the steps that need to be followed when an agent wants to isolate itself from the series connection in the converter. The flowchart for the isolation procedure is presented on the left part of Figure 5.

### 4.1 | Voltage reference adaptation

As the working of the stacked polyphase bridge converter is inherently unstable in motoring mode, it is of uttermost importance that the voltage balancing remains guaranteed before, during and after the isolation and reactivation of an agent. The first step of the isolation procedure for an agent is therefore to ensure that the voltage references  $\bar{v}_{dc,x}$  for the voltage balancers (4) are generated correctly. When agent  $r$  isolates itself from the series connection, the total dc-bus voltage  $E_{dc}$  must be divided over the remaining active agents, that is, the reference voltage generated by the dynamic average consensus algorithm of Section 3.1 should evolve from  $E_{dc}/p$  (with  $p$  the total number of agents, including the isolating ones) towards  $E_{dc}/p_{act}$  (with  $p_{act}$  the number of active agents only). Therefore, it is required to remove the local voltage measurement  $v_{dc,r}$  from (1) by adapting it according to (3): when an agent is not active, its input to its own dynamic average consensus algorithm is altered to the average value of the dynamic average consensus algorithm outputs  $\bar{v}_{dc,r-1}$  and  $\bar{v}_{dc,r+1}$  of its two neighbouring agents.

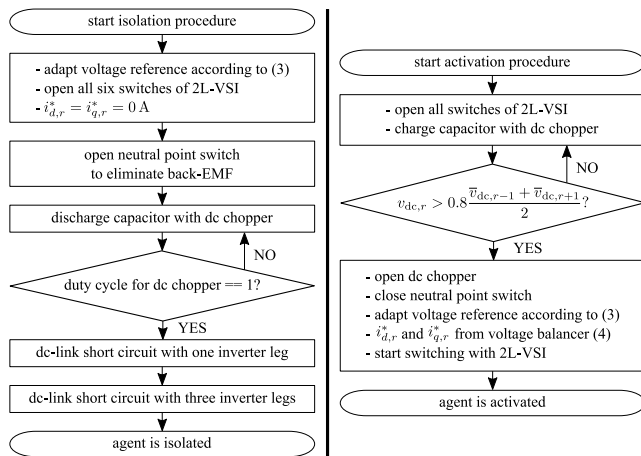


**FIGURE 5** Flowchart of the isolation (left) and activation (right) procedure.

## 4.2 | Back-EMF elimination

The back-EMF must be eliminated before lowering the dc-link voltage to avoid rectification over the anti-parallel diodes of the 2L-VSI. This is accomplished by means of the neutral point switch indicated in Figure 3. The neutral point switch is capable of opening and closing the neutral point of the wye-connected three-phase winding set of an agent. It comprises a three-phase diode rectifier, which rectifies the three ac-currents of the windings. As a result, only one additional unidirectional, active switch is required to interrupt the current path in the three windings of an agent, or to re-close its neutral point. However, to avoid large voltage spikes over this active switch, the currents in the agent's windings must be zero before the neutral point switch can be opened. To de-energise the windings, all six active switches of the 2L-VSI of the agent are opened, allowing the remaining inductive currents to die out over the anti-parallel diodes of the inverter legs, as illustrated in Figure 6. Once the currents in the three windings are zero, the neutral point switch can be opened safely. As long as the 2L-VSI of agent  $r$  is not switching, its current references  $i_{d,r}^*$  and  $i_{q,r}^*$  are set equal to zero.

### 4.3 | Controlled capacitor discharge

As long as there are active agents in the converter, the dc-link current  $i_{dc}$  keeps flowing through the series connection. Since an isolated agent does not inject current in its machine windings anymore (as previously explained in Section 4.2), this dc-current has to flow through the capacitor of the isolated agent, resulting in a rapid increase of its capacitor voltage in motoring mode. However, when an agent is isolated from the series connection in the converter, the intention is to decrease the capacitor voltage of this agent towards zero. Two requirements need to be satisfied for this purpose: the dc-link current  $i_{dc}$  must have an alternative current path through the isolated agent, and the capacitor of the isolated agent must be discharged. A dc chopper is able to fulfil these two requirements. It is indicated in Figure 3, and consists of a high power resistor and a controlled semiconductor switch.

When the dc chopper switch is closed, the capacitor can discharge, as is shown on the left side of Figure 7. The capacitor discharge current  $i_{C_r}$  and the dc-link current  $i_{dc}$  can flow through the resistor in this case. When the dc chopper switch is opened, the dc-link current flows through the capacitor, causing the capacitor voltage to increase. By controlling the duty cycle of the chopper switch, the relative duration of the capacitor

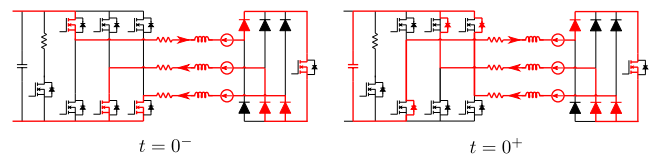


**FIGURE 6** Example of the phase current paths during normal operation at  $t = 0^-$ , and when the switches of the 2L-VSI are all opened at  $t = 0^+$ .

charging and discharging can be regulated. Consequently, the voltage  $v_{dc,r}$  over the capacitor can be controlled. A PI controller with parameters  $K_{p,rec}$  and  $K_{i,rec}$  is used to determine the duty cycle for the dc chopper switch, and a linear discharge curve is followed. The discharge curve has a predetermined slope  $s$ , and its starting voltage is equal to the measured capacitor voltage  $v_{dc,r}$  at the beginning of this step.

The capacitor voltage  $v_{dc,r}$  cannot drop below the voltage over the dc chopper resistor  $Ri_{dc}$ . To minimise this voltage drop, the resistance  $R$  should be chosen sufficiently small. However, a lower resistance  $R$  means larger currents through the dc chopper switch as well. The choice of the resistance  $R$  is hence a trade-off.

#### 4.4 | DC-link short circuit

As mentioned at the end of Section 4.3, the dc chopper cannot decrease the capacitor voltage of an isolated agent below  $Ri_{dc}$ , even when the dc chopper switch is always closed. Hence, the final step in the isolation procedure is to provide a low-impedance current path for the dc-link current  $i_{dc}$ . This low-impedance path can be formed by means of the switches of the 2L-VSI of the isolated agent (in case they are healthy). To avoid large currents when the remaining charge in the capacitor is discharged in the on-state resistances  $R_{on}$  of the inverter switches, only one inverter leg is closed first, as can be seen on the left side of Figure 8. The impedance of the current path is hence equal to  $2R_{on}$ . One sample period  $T_s$  later, all three inverter legs can be closed, as is illustrated on the right side of Figure 8, to minimise the impedance of the current path further to  $2R_{on}/3$ .

### 5 | AGENT ACTIVATION

When an agents wants to reactivate, a similar procedure can be followed as the one for agent isolation described in Section 4, but in the reverse direction. The flowchart for the activation procedure is presented on the right side of Figure 5. First, the

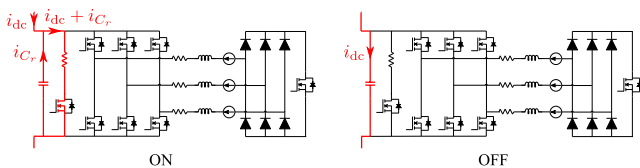


FIGURE 7 Current paths during the ON-state (left) and the OFF-state (right) of the dc chopper switch.

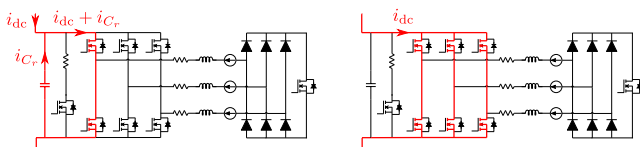


FIGURE 8 Current paths during the dc-link short circuit.

dc-link short circuit by means of the 2L-VSI switches is lifted. The dc-link current flows through the dc-link capacitor of the agent again, making the capacitor voltage to increase in motoring mode. The voltage can be increased according to a predefined charge curve by means of the dc chopper control elaborated upon in Section 4.3. When the capacitor voltage is sufficiently high, the dc chopper is deactivated (i.e. the duty cycle of the dc chopper switch is continuously zero), the neutral point switch is closed, the integral action of the current PI controller of the reactivated agent is reset, its 2L-VSI starts switching again and the normal operation of the agent can be resumed. The capacitor voltage is considered sufficiently high when it is higher than the rectified back-EMF voltage, and close to the reference voltage of its neighbours, that is, when  $v_{dc,r} > 0.8 \frac{\bar{v}_{dc,r-1} + \bar{v}_{dc,r+1}}{2}$ .

## 6 | CASE STUDY

In this paper, a multi-three-phase 4 kW segmented armature torus axial-flux permanent magnet synchronous machine with surface-mounted permanent magnets will serve as a case study. This modular motor drive consists of  $n = 15$  identical pole drive units, and hence  $p = 5$  agents. Its specifications are listed in Table 1. Although every agent can be equipped with a neutral point switch and dc chopper, only agent 5 has these additional hardware components at its disposal throughout this work. Therefore, only agent 5 is isolated and reactivated in this specific case study.

The performance of the proposed decentralised, dynamic dc-link reconfiguration strategy for motoring mode (including the dynamic average consensus algorithm of Section 3.1, the voltage balancer of Section 3.2, the current controller of Section 3.3 and the isolation and activation procedures of Sections 4 and 5) will be validated by both simulations and experimental results. The control parameters are summarised in Table 2. The case study is conducted at a constant mechanical speed  $N$  of 700 rpm, and a constant  $q$ -current reference  $i_{q,ref}$  of 7A.

### 6.1 | Simulation results

#### 6.1.1 | Methodology

The simulations are executed using Simscape™ in the MATLAB® & Simulink® R2019b environment, with the variable-step DAE solver for Simscape, and a maximum step size of  $1/(200f_s)$ . The AFPMSM is modelled by means of a custom-made Simscape block, based on a fifteen-phase state-space model in the  $abc$ -reference frame. The machine parameters (summarised in Table 1) are obtained by means of measurements on the test setup. The stacked polyphase bridge converter is modelled by means of standard Simscape building blocks, with parameters obtained from the datasheets of the components in the test setup. A representative level of white noise is added to the dc-link capacitor voltage signals, in order

to simulate the impact of measurement noise. It is assumed that the speed is kept perfectly constant at 700 rpm during the whole simulation.

**TABLE 1** Drive parameters.

Parameter	Symbol	Value
Rated torque (Nm)	$T_n$	15
Rated current (A)	$I_n$	11
Rated speed (rpm)	$N_n$	2500
Number of pole pairs	$N_p$	8
Stator winding resistance (m $\Omega$ )	$R_s$	65
Stator inductance ( $\mu$ H)	$L_d = L_q$	309.95
Self and mutual inductances ( $\mu$ H) ( $s \in \{1, 2, \dots, 15\}$ )	$L_{s,s}$	316.00
	$L_{s,s-1} = L_{s,s+1}$	111.00
	$L_{s,s-2} = L_{s,s+2}$	15.50
	$L_{s,s-3} = L_{s,s+3}$	9.52
	$L_{s,s-4} = L_{s,s+4}$	8.27
	$L_{s,s-5} = L_{s,s+5}$	6.05
	$L_{s,s-6} = L_{s,s+6}$	6.07
	$L_{s,s-7} = L_{s,s+7}$	5.31
Permanent magnet flux linkage (Wb)	$\Psi_m$	0.02
Total dc-bus voltage (V)	$E_{dc}$	240
DC-link capacitance per agent ( $\mu$ F)	$C$	220
Resistance dc chopper ( $\Omega$ )	$R$	1

**TABLE 2** Control parameters.

Parameter	Symbol	Value
Dynamic average consensus		
Update frequency of the voltage balancer (kHz)	$f_{vb}$	2
Filtering constant	$\alpha$	0.1
Convergence rate	$\rho$	0.6481
Proportional gain	$k_p$	1.6022
Integral gain	$k_i$	0.5093
Active voltage balancer		
Gain (1/V)	$g$	0.1
Maximum current limit (A)	$i_{max}$	10
Decentralised current control		
Sampling and switching frequency (kHz)	$f_s$	10
Proportional gain	$K_p$	2
Integral gain	$K_i$	200
Agent isolator/activator		
Proportional gain	$K_{p,rec}$	0.1
Integral gain	$K_{i,rec}$	0.5
Slope (V/s)	$s$	500

## 6.1.2 | Agent isolation

Figure 9 shows the simulation results for the isolation procedure. Until  $t = 2.5$  s, all agents are activated, and hence  $p_{act} = p = 5$ . The dynamic average consensus algorithm of each agent  $x$  is able to track the average of all the local capacitor voltage measurements  $\sum_{y=1}^p v_{dc,y}/p \approx E_{dc}/p = 240/5 = 48$  V correctly, and to provide this as a smooth voltage reference  $\bar{v}_{dc,x} = 48$  V.

As only agent 5 is equipped with a dc chopper and neutral point switch, its capacitor voltage  $v_{dc,5}$  is slightly lower than the capacitor voltages over the other agents, due to the forward voltage drop of the diodes in the neutral point switch. Its voltage balancer (4) limits this voltage deviation by decreasing the original  $q$ -current reference  $i_{q,ref}$  of 7 A to  $i_{q,5}^* = 5.8$  A. As the modular AFPMSM used as a case study throughout this paper has surface-mounted permanent magnets (i.e.  $L_d \approx L_q$ ), and no field-weakening is considered,  $i_{d,ref}$  is constantly zero,

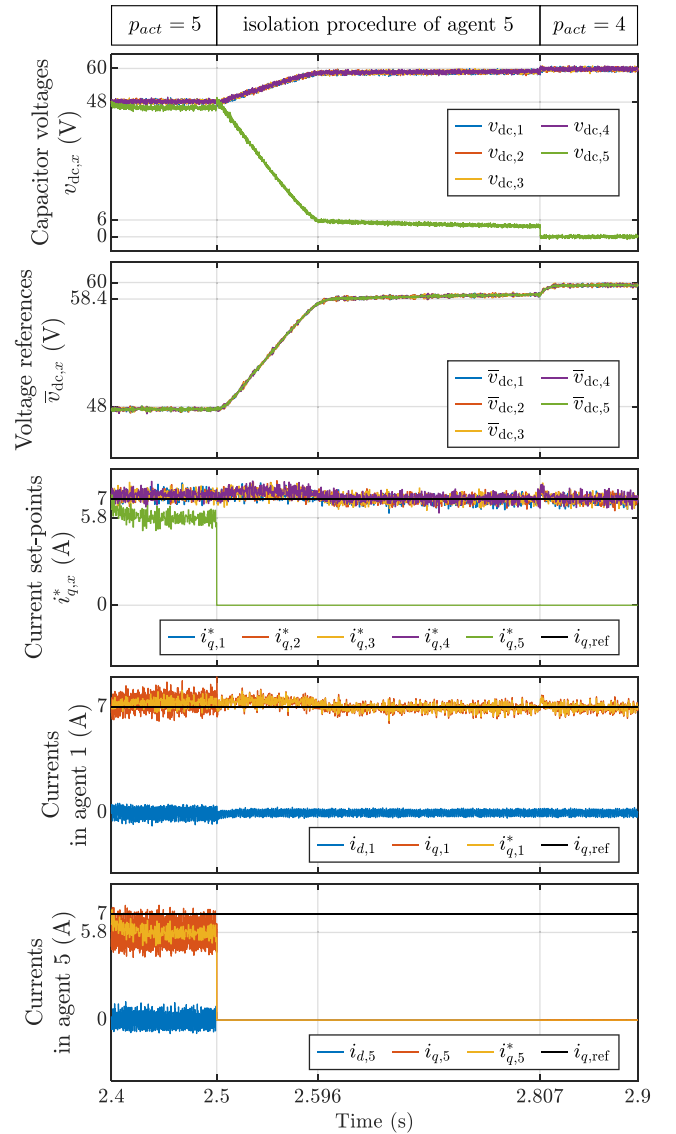


**FIGURE 9** Simulation results. Agent 5 is isolated at  $t = 2.5$  s.

and hence  $i_{d,x}^* = 0$  A as well. However, when field-weakening would be applied, the voltage balancer (4) would influence the  $d$ -current reference as well. The decentralised current controllers are able to track the current set-points  $i_{d,x}^*$  and  $i_{q,x}^*$  well.

At  $t = 2.5$  s, agent 5 receives an external command to start its isolation procedure. Agent 5 immediately opens all six switches of its 2L-VSI, adapts its voltage reference generation to the inactive state according to (3) and sets its current set-points  $i_{d,5}^*$  and  $i_{q,5}^*$  equal to 0 A. The current components  $i_{d,5}$  and  $i_{q,5}$  die out immediately. In the next sampling period  $T_s$ , agent 5 opens its neutral point switch, to eliminate its back-EMF. During these two sample periods, the capacitor voltage  $v_{dc,5}$  rises uncontrollably, due to the dc-link current  $i_{dc}$  that has no other path to flow through than the dc-link capacitor of agent 5. However, in the next period  $T_s$ , agent 5 determines its capacitor discharge curve, and starts regulating the duty cycle of the dc chopper switch in order to follow this curve. The capacitor voltage  $v_{dc,5}$  indeed decreases at a rate  $s$  of 500 V/s, as can be seen in Figure 9:  $48/500 = 0.096$  s later,  $v_{dc,5}$  has decreased towards 6 V. At this point, the relative importance of the voltage drop  $Ri_{dc}$  over the resistor of the dc chopper is considerable, and changing the duty cycle of the dc chopper switch only has limited effect on  $v_{dc,5}$ . The integral action of the PI controller of the dc chopper keeps increasing, until the dc chopper's duty cycle equals one. At this point, which occurs at  $t = 2.807$  s, the dc chopper cannot further decrease  $v_{dc,5}$  anymore, and the dc-link is short-circuited by means of the 2L-VSI switches, as discussed in Section 4.4. Agent 5 is then completely isolated.

It must be noted that during the entire isolation procedure, the dynamic average consensus algorithm of Section 3.1 correctly tracks the average capacitor voltage over the remaining four active agents. Also, the voltage balancers of Section 3.2 of these active agents are able to follow the reference voltage coming from their consensus algorithm. The complete isolation procedure takes approximately 0.307 s to finish. However, the majority of the dc-link changes have already taken place after 0.096 s.

### 6.1.3 | Agent activation

Figure 10 shows the simulation results for the activation procedure. Until  $t = 7.5$  s, agent 5 is isolated, and hence  $p_{act} = 4$ . Hence, the capacitor voltages of the four remaining active agents are regulated towards  $E_{dc}/p_{act} = 240/4 = 60$  V.

At  $t = 7.5$  s, agent 5 receives an external command to start its reactivation procedure. It immediately undoes its dc-link short circuit by reopening the six switches of its own 2L-VSI, and starts regulating the duty cycle of its dc chopper to follow its capacitor recharge curve. The capacitor voltage  $v_{dc,5}$  indeed increases with a slope  $s = 500$  V/s, until it reaches 80% of the value of the reference voltage of its neighbours at  $t = 7.579$  s. In the meantime, the capacitor voltages of the four active agents  $v_{dc,x}$  ( $x \in \{1, 2, 3, 4\}$ ) decrease towards 48 V again, as do their references  $\bar{v}_{dc,x}$ . At  $t = 7.579$  s, the switch of

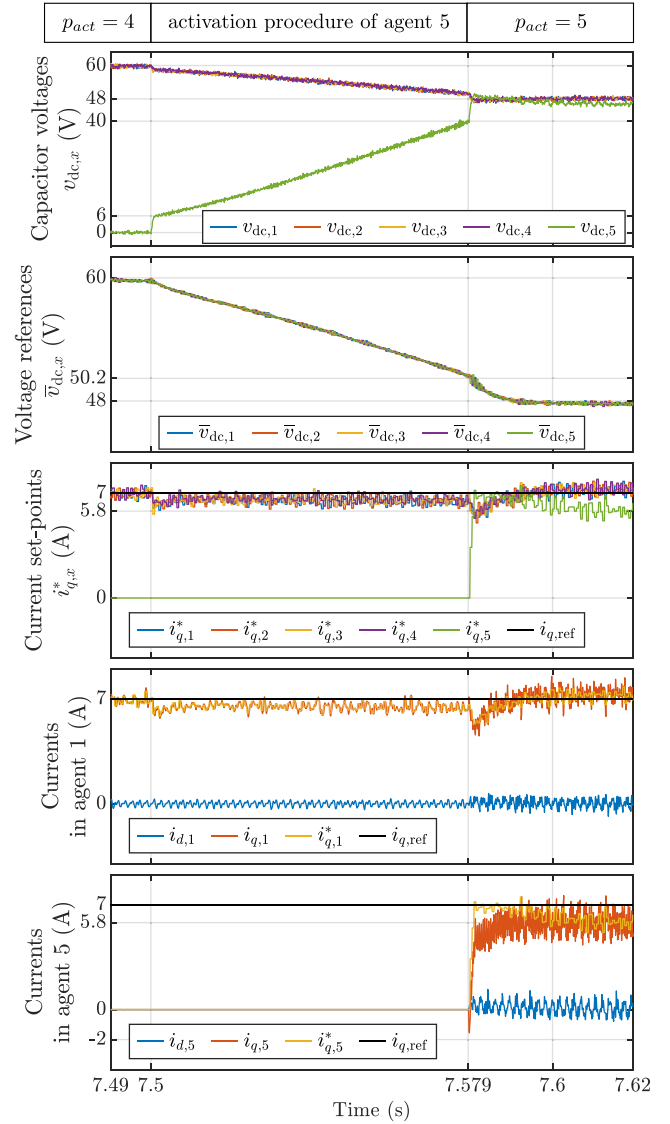


FIGURE 10 Simulation results. Agent 5 is reactivated at  $t = 7.5$  s.

the dc chopper of agent 5 is opened again. Its neutral point switch is closed, and the normal operation of agent 5 is resumed. This means that its voltage reference is generated according to the active state in (3) again, its current set-points  $i_{d,5}^*$  and  $i_{q,5}^*$  are coming from its voltage balancer (4), and the 2L-VSI switches according to the duty cycles generated by the PI current controller. The resumption of the normal activity of agent 5 results in slight current and voltage transients, which have died out at  $t = 7.6$  s. The complete reactivation procedure hence takes 0.1 s to finish.

## 6.2 | Experimental validation

### 6.2.1 | Test setup

The 4 kW segmented armature torus AFPMSM of the test setup is depicted in Figure 11. It is working in motoring mode,



while its mechanical speed is imposed by means of an induction load motor. The torque  $T_{em}$  is measured with a Lorenz DR-2112 torque transducer mounted on the shaft between the AFPMSM and the load motor. The AFPMSM consists of 15 identical motor modules, grouped into five three-phase agents. It is fed by means of a modular low-voltage scalable power platform from Infineon, which comprises three PE modules per agent. The five agents are connected in series to a single dc power supply. Each agent is completed with a set of three LEM LA 25-P current transducers, a dc-link capacitor and a voltage sensor. Agent 5 is also equipped with a dc chopper and neutral point switch, using the same OptiMOS™3 power-transistors and 2EDL23 gate drivers as for the Infineon PE modules. As the high-side switches of the PE modules are driven by bootstrap circuits, it is not possible to validate the dc-link short circuit explained in Section 4.4 on the test setup.

Although the controllers of the five agents are completely decentralised, requiring only the communication of  $p_x$  and  $\bar{v}_{dc,x}$  between neighbouring agents as depicted in Figure 4, they are still implemented on the FPGA of a single MicroLabBox. In this way, the communication frequency  $f_{vb}$  between the agents is not restricted by a specific communication protocol. The effect of  $f_{vb}$  is discussed in Section 7. The controllers are built on the FPGA of the dSPACE MicroLabBox using the RTI FPGA Programming Blockset (Version 3.10.1), which requires dSPACE (release 2020-B), the Xilinx System Generator for DSP Blockset and Xilinx Vivado 2020.1.

The measurement results are drawn and recorded from the MicroLabBox by means of ControlDesk software at a sampling rate of 10 kHz.

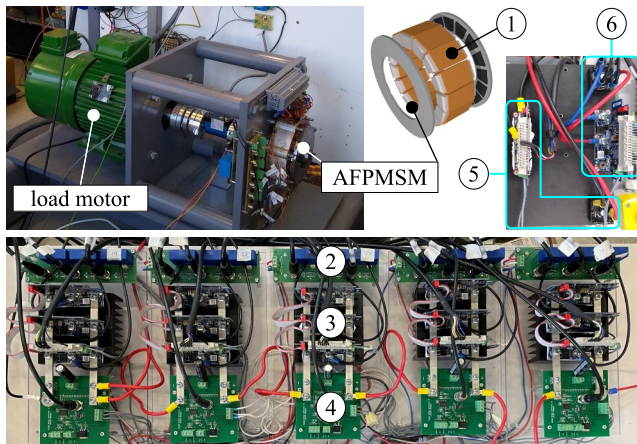


**FIGURE 11** Test setup consisting of an induction load motor and (1) a modular 4 kW AFPMSM with 15 motor modules. Each motor module comprises a stator core with its concentrated winding. The motor modules are grouped into five three-phase agents, with five separate neutral points. Each agent is equipped with (2) a set of three current sensors, (3) and a dedicated three-phase 2L-VSI (4) with its own 220  $\mu$ F dc-link capacitor and voltage sensor. All agents are connected in series to the same dc power supply, in order to form a stacked polyphase bridge converter. Agent 5 is also equipped with (5) a dc chopper, and (6) a neutral point switch. The dc chopper consists of a power MOSFET in series with a resistor, connected in parallel to the 2L-VSI of agent 5. The neutral point switch comprises a three-phase diode rectifier and a power MOSFET. It is connected to the three power terminals of agent 5 that can form its neutral point.

## 6.2.2 | Experimental results

The measured results of Figure 12 show that agent 5 can repeatedly be isolated and reactivated. As the  $q$ -current reference  $i_{q,ref}$  of all the agents is kept constant at a value of 7 A, the isolation of agent 5 reduces the torque by a factor of 4/5. The

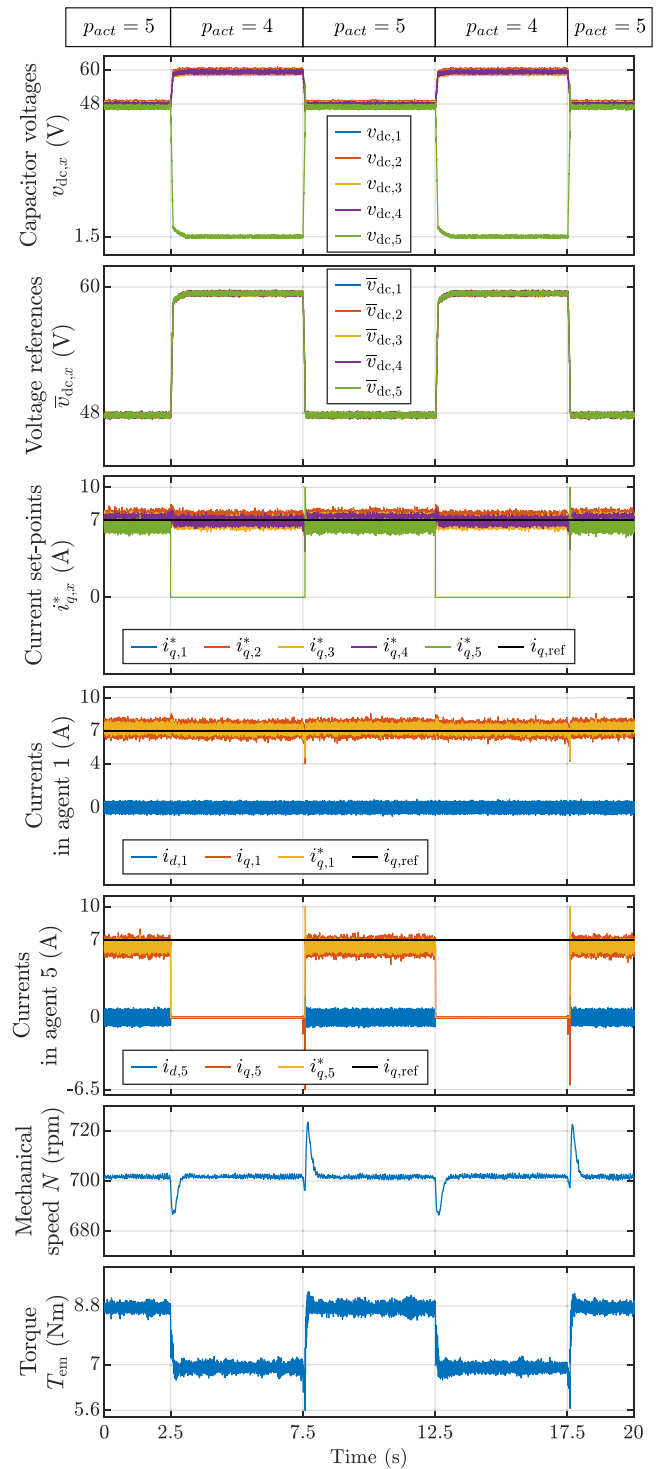


**FIGURE 12** Experimental results. Agent 5 is isolated at  $t = 2.5$  s and  $t = 12.5$  s, and reactivated at  $t = 7.5$  s and  $t = 17.5$  s.

torque changes result in small speed disturbances. However, it must be noted that the torque is never interrupted, neither during the isolation nor the reactivation of agent 5.

Figure 13 presents a more detailed view of the experimental results during the isolation procedure of agent 5. The results are in good agreement with the simulations provided in Figure 9, apart from the fact that the dc-link short circuit could not be conducted on the test setup at  $t = 3.053$  s (when the dc chopper's duty cycle equals one, and the dc chopper cannot reduce  $v_{dc,5}$  any further), due to the bootstrap circuits in the 2L-VSI. The experimental validation confirms that the majority of the dc-link changes have already taken place after 0.096 s.

A more detailed view of the reactivation procedure of agent 5 is presented in Figure 14. The experimental results are again in good agreement with the simulation results of Figure 10. However, the resumption of the normal operation of agent 5 at  $t = 7.579$  s is accompanied by more pronounced current and voltage transients than anticipated by

the simulation results. However, these transients have died out after 0.1 s, just as was expected from the simulation results.

## 7 | INFLUENCE OF THE COMMUNICATION FREQUENCY

The communication frequency  $f_{vb}$  (which is also the frequency at which the dynamic average consensus algorithm of Section 3.1 and the active voltage balancing algorithm of Section 3.2 are executed) does not need to be related with the sampling frequency  $f_s$  of the decentralised current controllers of Section 3.3. As a result, the communication frequency  $f_{vb}$  can be lower than the sampling frequency  $f_s$  (which is set equal to 10 kHz), in order to enable the use of state-of-the-art communication protocols [30]. Figure 15 illustrates the experimentally obtained effect of  $f_{vb}$  on the reconfiguration

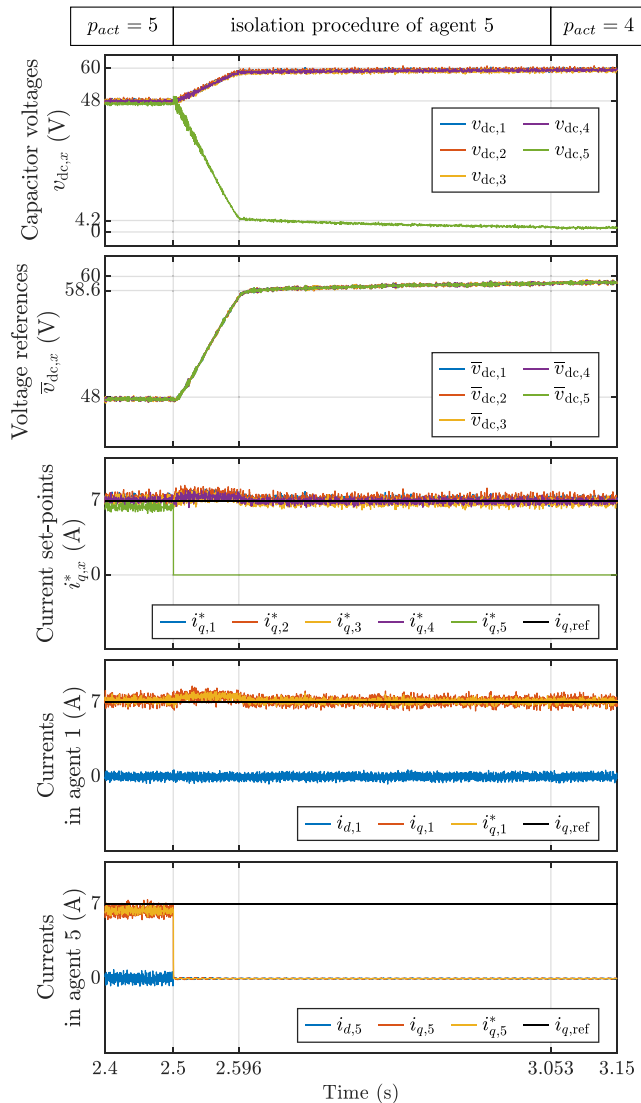


FIGURE 13 Experimental results. Agent 5 is isolated at  $t = 2.5$  s.

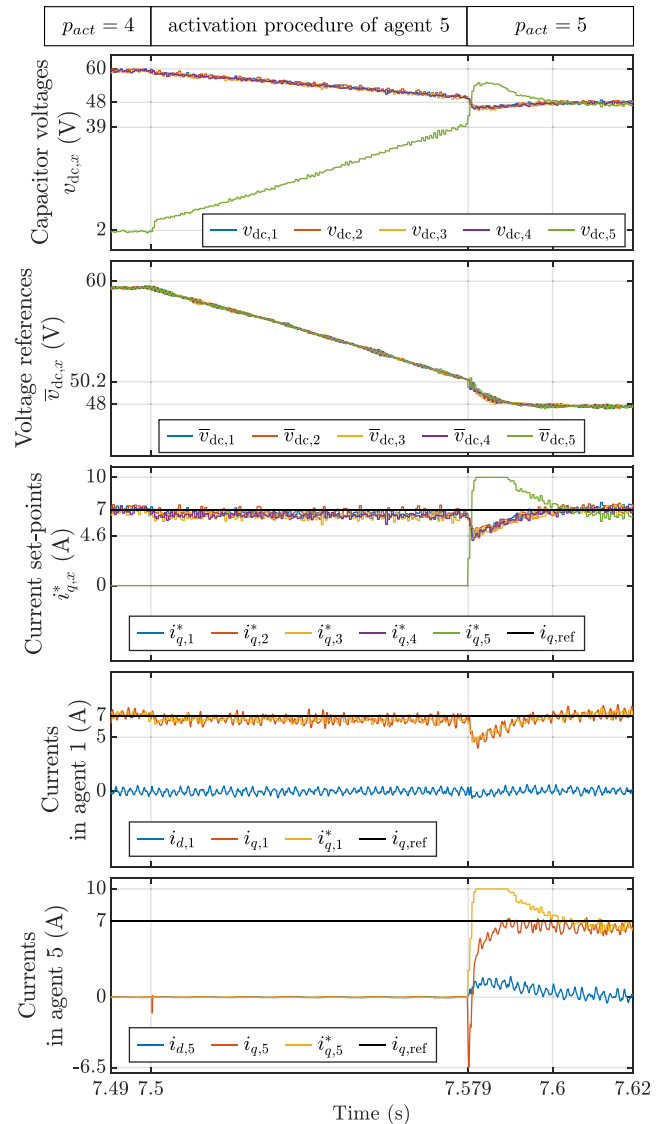
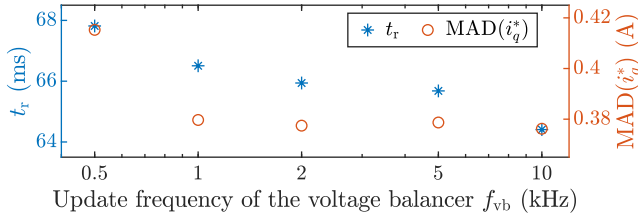


FIGURE 14 Experimental results. Agent 5 is reactivated at  $t = 7.5$  s.



**FIGURE 15** Measured effect of the communication frequency  $f_{vb}$  on the reconfiguration time  $t_r$  and the current set-point ripple  $MAD(i_q^*)$ .

dynamics, and the ripple generated in the  $q$ -current set-points. The impact is parametrised by means of the reconfiguration time  $t_r$ , and the mean absolute deviation (MAD) of the current set-points  $i_{q,x}^*$  from their initial reference  $i_{q,ref}$ . The parameter  $t_r$  is defined as the average of two time periods:

- the time period during which the voltage  $v_{dc,5}$  is decreasing at a rate  $s$  when agent 5 is isolated (which corresponds to the period between the start of the isolation at  $t = 2.5$  s, and the knee point in  $v_{dc,5}$  at  $t = 2.596$  s in Figure 13);
- the time period that is required for the convergence of all the capacitor voltages  $v_{dc,x}$  after the reactivation of agent 5 (which corresponds to the period between  $t = 7.5$  s and  $t = 7.6$  s in Figure 14).

The parameter  $MAD(i_q^*)$  is computed as the average of the parameters  $MAD(i_{q,x}^*)$  of all the agents  $x \in \{1, \dots, 5\}$ :

$$MAD(i_{q,x}^*) = \frac{\sum_Z |i_{q,ref} - i_{q,x}^*|}{Z}, \quad (5)$$

with  $Z$  the number of samples used for the calculation. The values depicted in Figure 15 are averaged over three different operating points (i.e.  $[E_{dc} = 75 \text{ V}, i_{q,ref} = 3 \text{ A}, N = 200 \text{ rpm}]$ ,  $[E_{dc} = 175 \text{ V}, i_{q,ref} = 3 \text{ A}, N = 200 \text{ rpm}]$  and  $[E_{dc} = 240 \text{ V}, i_{q,ref} = 7 \text{ A}, N = 400 \text{ rpm}]$ ). The fact that  $E_{dc}$  is lower than 240 V in two of these three operating points (while the slope  $s$  remains equal to 500 V/s) reduces the reconfiguration time  $t_r$  for  $f_{vb} = 2$  kHz to less than the 100 ms that are observed in the experimental results of Figures 13 and 14.

In general, it can be concluded that both the reconfiguration time and the ripple in the  $q$ -current set-points increase when the communication frequency is lowered. Indeed, when  $f_{vb}$  is lower, the capacitor voltages have more time to diverge in between two updates of the voltage balancer, and hence more time and a larger control effort are required to stabilise them again.

## 8 | CONCLUSION AND FUTURE WORK

A modular motor drive fed by a stacked polyphase bridge converter comprises multiple three-phase agents, each consisting of a three-phase winding set, a 2L-VSI and a dedicated

controller. The agents can communicate by means of a ring network, and they are all connected in series to a single dc voltage source. This type of drive still faced the challenge that a faulty agent could not be isolated from the series connection in motoring mode, and that the limited dc-link voltage per agent imposed a limit on the speed. Therefore, a multi-agent dc-bus reconfiguration strategy was proposed in this paper, which allows the agents to isolate and reactivate themselves in the series connection. For this purpose, the hardware needed to be extended with only two active unidirectional switches per agent: a neutral point switch to eliminate the back-EMF during isolation, and a dc chopper for controlled capacitor discharging and recharging. Besides the hardware alterations, also the control strategy was discussed. The dedicated controller of each agent comprised a dynamic average consensus algorithm, an autonomous voltage balancer and a decentralised PI current controller to keep the dc-link voltages stable, even during reconfiguration and motoring mode. The benefits of this control strategy include that only local measurements and computations are required. The control is hence completely decentralised and easily scalable. Both simulations and measurements on a 4 kW test setup demonstrated that dc-bus reconfiguration is feasible with the proposed strategy. They confirmed that the dc-bus can be reconfigured in 100 ms, without torque interruption.

In future work, the control strategy can still be further developed to allow the agents to isolate or reactivate themselves based on their health status or the operating point. Furthermore, the multi-agent control strategy can be extended to let the agents automatically redistribute the torque demand among the active agents only, hence avoiding a decrease in torque when an agent is isolated, or an increase in torque when an agent is reactivated.

## NOMENCLATURE

2L-VSI	two-level voltage source inverter
(AF)PMSM	axial-flux permanent magnet synchronous machine
back-EMF	back electromotive force
MMD	modular motor drive
PDU	pole drive unit
PE	power electronic
$\alpha$	filtering constant
$C$	dc-link capacitance per agent
$E_{dc}$	total dc-link voltage
$f_{vb}$	update frequency of the voltage balancer
$f_s$	sampling and switching frequency
$g$	gain of the active voltage balancer
$i_{Cr}$	capacitor discharge current
$i_{d,ref}, i_{q,ref}$	original current component references from the user
$i_{d,x}, i_{q,x}$	current components of agent $x$
$i_{d,x}^*, i_{q,x}^*$	current component set-points for agent $x$ after the voltage balancer
$i_{max}$	maximum current limit
$k$	discrete time instant (with $T_{vb}$ between subsequent time instants)

$k_i$	integral gain of the dynamic average consensus algorithm
$K_i$	integral gain of the decentralised current controller
$K_{i,rec}$	integral gain of the agent isolator/activator
$k_p$	proportional gain of the dynamic average consensus algorithm
$K_p$	proportional gain of the decentralised current controller
$K_{p,rec}$	proportional gain of the agent isolator/activator
$L_d, L_q$	stator winding inductances
$n$	number of pole drive units
$N$	mechanical speed
$\omega$	electrical rotor speed
$\Psi_m$	permanent magnet flux linkage
$p$	number of agents
$p_{act}$	number of active agents
$p_x$	internal state variable of the dynamic average consensus algorithm of agent $x$
$q_x$	internal state variable of the dynamic average consensus algorithm of agent $x$
$\rho$	convergence rate of the dynamic average consensus algorithm
$r$	agent that is isolated or activated
$R$	dc chopper resistance
$R_s$	stator winding resistance
$R_{on}$	on-state resistance of the inverter switches
$s$	slope of the linear capacitor discharge curve
$t$	continuous time instant
$T_s$	sample period
$T_{vb}$	update period of the voltage balancer
$v_{dc,x}$	dc-link capacitor voltage of agent $x$
$\bar{v}_{dc,x}$	capacitor voltage reference of agent $x$
$v_{dc,x,f}$	filtered voltage input for the dynamic average consensus algorithm of agent $x$
$v_x$	voltage input for the dynamic average consensus algorithm of agent $x$

## AUTHOR CONTRIBUTIONS

**Lynn Verkroost:** Conceptualisation; Formal analysis; Investigation; Methodology; Software; Validation; Visualisation; Writing – original draft. **Alexander Vande Ghinste:** Formal analysis; Investigation; Software; Validation; Writing – review & editing. **Lorrana Faria da Rocha:** Conceptualisation. **Jeroen D. M. De Kooning:** Conceptualisation; Supervision; Writing – review & editing. **Frederik De Belie:** Supervision; Writing – review & editing. **Peter Sergeant:** Funding acquisition; Project administration; Resources; Supervision; Writing – review & editing. **Pal Keim Olsen:** Conceptualisation. **Hendrik Vansompel:** Conceptualisation; Funding acquisition; Project administration; Resources; Supervision; Validation; Writing – review & editing.

## CONFLICT OF INTEREST STATEMENT

None.

## DATA AVAILABILITY STATEMENT

The data that support the findings of this study are available from the corresponding author upon reasonable request.

## ORCID

Lynn Verkroost  <https://orcid.org/0000-0002-1442-677X>  
 Jeroen D. M. De Kooning  <https://orcid.org/0000-0002-0358-4350>

## REFERENCES

1. Abebe, R., et al.: Integrated motor drives: state of the art and future trends. *IET Electr. Power Appl.* 10(8), 757–771 (2016). <https://doi.org/10.1049/iet-epa.2015.0506>
2. Verkroost, L., et al.: Simultaneous DC-link and stator current ripple reduction with interleaved carriers in multiphase controlled integrated modular motor drives. *IEEE Trans. Ind. Electron.* 68(7), 5616–5625 (2021). <https://doi.org/10.1109/tie.2020.2992965>
3. Mohamed, A.H., Vansompel, H., Sergeant, P.: Reconfigurable modular fault-tolerant converter topology for switched reluctance motors. *IEEE J. Emerg. Sel Topics in Power Electronics* 10(3), 2890–2902 (2022). <https://doi.org/10.1109/jestpe.2021.3130124>
4. Rubino, S., et al.: Modular vector control of multi-three-phase permanent magnet synchronous motors. *IEEE Trans. Ind. Electron.* 68(10), 9136–9147 (2021). <https://doi.org/10.1109/tie.2020.3026271>
5. Wen, Z., et al.: Modular power sharing control for bearingless multithree phase permanent magnet synchronous machine. *IEEE Trans. Ind. Electron.* 69(7), 6600–6610 (2022). <https://doi.org/10.1109/tie.2021.3097610>
6. Prieto-Araujo, E., et al.: Decentralized control of a nine-phase permanent magnet generator for offshore wind turbines. *IEEE Trans. Energy Convers.* 30(3), 1103–1112 (2015). <https://doi.org/10.1109/tec.2015.2412550>
7. Liang, G., et al.: An enhanced distributed control architecture of multiple three-phase PMSG for improving redundancy. *IEEE Trans. Power Electron.* 38(9), 11338–11351 (2023). <https://doi.org/10.1109/tpel.2023.3288049>
8. Verkroost, L., et al.: Multi-agent position estimation in modular motor drives using low-resolution sensors. *IEEE Open Journal of the Industrial Electronics Society* 3, 105–115 (2022). <https://doi.org/10.1109/ojies.2022.3146302>
9. Verkroost, L., et al.: Multi-agent control in modular motor drives by means of gossip consensus. *IET Electr. Power Appl.* 16(4), 483–497 (2022). <https://doi.org/10.1049/elp2.12170>
10. Verkroost, L., et al.: Multiagent control in modular motor drives by means of deterministic consensus. *IEEE Trans. Ind. Electron.* 70(2), 1205–1215 (2023). <https://doi.org/10.1109/tie.2022.3163504>
11. Duran, M.J., et al.: Multiphase energy conversion systems connected to microgrids with unequal power-sharing capability. *IEEE Trans. Energy Convers.* 32(4), 1386–1395 (2017). <https://doi.org/10.1109/tec.2017.2721499>
12. Che, H.S., et al.: Operation of a six-phase induction machine using series-connected machine-side converters. *IEEE Trans. Ind. Electron.* 61(1), 164–176 (2014). <https://doi.org/10.1109/tie.2013.2248338>
13. Verkroost, L., et al.: Multi-agent Voltage Balancing in Modular Motor Drives with Series-Connected Power Electronic Converters. *IET Power Electron.* (2023)
14. Nikouie, M., et al.: DC-link stability analysis and controller design for the stacked polyphase bridges converter. *IEEE Trans. Power Electron.* 32(2), 1666–1674 (2017). <https://doi.org/10.1109/tpel.2016.2553129>
15. Jin, L., et al.: Modulation and power losses of a stacked polyphase bridge converter. *IEEE J. Emerg. Sel Topics in Power Electronics* 5(1), 409–418 (2017). <https://doi.org/10.1109/jestpe.2016.2621349>
16. Yildirim, B., et al.: Efficiency optimized power-sharing algorithm for modular battery energy storage systems. *IEEE Trans. Ind. Electron.* 70(11), 11299–11309 (2023). <https://doi.org/10.1109/tie.2022.3229311>



17. Gjerde, S.S., et al.: Control and fault handling in a modular series-connected converter for a transformerless 100 kV low-weight offshore wind turbine. *IEEE Trans. Ind. Appl.* 50(2), 1094–1105 (2014). <https://doi.org/10.1109/tia.2013.2272032>
18. Norrga, S., et al.: A novel inverter topology for compact EV and HEV drive systems. In: *IECON 2013 - 39th Annual Conference of the IEEE Industrial Electronics Society*, pp. 6590–6595 (2013)
19. Khalili, M., et al.: Optimal instantaneous prediction of voltage instability due to transient faults in power networks taking into account the dynamic effect of generators. *Cogent Engineering* 9(1), 2072568 (2022). [Online]. Available: <https://doi.org/10.1080/23311916.2022.2072568>
20. Zoric, I., Jones, M., Levi, E.: Voltage balancing control of a symmetrical nine-phase machine with series-connected DC links. In: *2017 IEEE 26th International Symposium on Industrial Electronics (ISIE)*, pp. 1052–1057 (2017)
21. Yang, H., Zhang, Y., Shen, W.: Predictive current control and field-weakening operation of SPMSM drives without motor parameters and DC voltage. *IEEE J. Emerg. Sel Topics in Power Electronics* 10(5), 5635–5646 (2022). <https://doi.org/10.1109/jestpe.2022.3167273>
22. Gashtil, H., et al.: Closed-loop voltage control for maximizing inverter output voltage in the field weakening region of induction machines. *IEEE J. Emerg. Sel Topics in Power Electronics* 10(6), 7514–7526 (2022). <https://doi.org/10.1109/jestpe.2022.3192120>
23. Jayarajan, R., Fernando, N., Nutkani, I.U.: A review on variable flux machine technology: topologies, control strategies and magnetic materials. *IEEE Access* 7, 70141–70156 (2019). <https://doi.org/10.1109/access.2019.2918953>
24. Liu, W., et al.: Loss-reduction-oriented optimization methodology of hybrid-magnetic-circuit variable flux memory machine for global efficiency improvement. *IEEE J. Emerg. Sel Topics in Power Electronics* 10(2), 1658–1670 (2022). <https://doi.org/10.1109/jestpe.2021.3065032>
25. Huang, H., Chang, L.: Electrical two-speed propulsion by motor winding switching and its control strategies for electric vehicles. *IEEE Trans. Veh. Technol.* 48(2), 607–618 (1999). <https://doi.org/10.1109/25.752586>
26. Li, A., et al.: Online drive topology conversion technology for PMSM speed range extension. *IEEE Trans. Power Electron.* 37(6), 7113–7121 (2022). <https://doi.org/10.1109/tpel.2022.3140184>
27. “Bugatti Veyron 16.4 Super Sport - Technical Specifications,” Bugatti. [Online]. [https://www.bugatti.com/fileadmin/media/Media/Veyron/Super\\_Sport/Techni%20cal\\_Specifications\\_Bugatti\\_Veyron\\_16.4\\_Super\\_Sport.pdf](https://www.bugatti.com/fileadmin/media/Media/Veyron/Super_Sport/Techni%20cal_Specifications_Bugatti_Veyron_16.4_Super_Sport.pdf)
28. Van Scoy, B., Freeman, R.A., Lynch, K.M.: Design of robust dynamic average consensus estimators. In: *2015 54th IEEE Conference on Decision and Control (CDC)*, pp. 6269–6275 (2015)
29. Kia, S.S., et al.: Tutorial on dynamic average consensus: the problem, its applications, and the algorithms. *IEEE Control Syst. Mag.* 39(3), 40–72 (2019). <https://doi.org/10.1109/mcs.2019.2900783>
30. Savi, F., et al.: Information technologies for distributed machine drives: an overview. In: *2019 IEEE International Electric Machines & Drives Conference (IEMDC)*, pp. 1805–1809 (2019)

**How to cite this article:** Verkroost, L., et al.: Dynamic multi-agent dc-bus reconfiguration in modular motor drives with a stacked polyphase bridge converter. *IET Electr. Power Appl.* 1–14 (2023). <https://doi.org/10.1049/elp2.12376>